journal

J. Am. Ceram. Soc., 89 [4] 1257–1265 (2006)
DOI: 10.1111/j.1551-2916.2005.00889.x
© 2006 The American Ceramic Society

Simulation of Colloidal Particle Packing for Photonic Bandgap Crystals

Jenn-Feng Li and Chuin-Shan Chen†

Department of Civil Engineering, National Taiwan University, Taipei 106, Taiwan

Bang-Ying Yu and Wen-Cheng J. Wei*

Department of Materials Science and Engineering, National Taiwan University, Taipei 106, Taiwan

We study the packing history and packing structures of photonic bandgap crystals consisting of mono-sized SiO_2 particles. Simulations with combined actions of Brownian motion, inter-particle interactions, and imposed external fields are considered. Numerical tactics to support modeling of Brownian particle agglomerations and consolidation and drying processing are developed. Our results suggest that the desired close-packed patterns on the surface are propagated from those at the bottom layer during consolidation. The driving forces for this pattern formation and growth are the coupling between inter-particle interactions and constraints from imposed external fields.

I. Introduction

PHOTONIC bandgap (PBG) crystals consist of periodical assemblies of mono-sized ceramic particles. The particle sizes are around several 100 nm, whose length scale is proportional to the wavelength of light in the band gap.[1] To fabricate PBG crystals, colloidal processing is often utilized in which the formation of packing structures results from sedimentation of particles in suspensions.[2,3] An outstanding issue on synthesis of PBG crystals is thus the ability to fabricate desired packing structures so that light can be controlled.[4] Trau *et al.*[5] manipulated various particle clusters by an ultrasonic wave, which induced a lateral attraction motion to assemble micro-sized silica particles to an ordered two dimensional (2D) structure. Sarkar *et al.*[6] found that formation of monolayer silica particles was similar to the atomic film growth via molecular-beam epitaxy. Two growth processes were observed. In the early stage, the behavior of colloidal particles was similar to diffusion-limited aggregation. It then transferred to the stage of consolidation inside the cluster. In addition to bulky PBG crystals, Masuda *et al.*[7] developed a process to fabricate wires by self-assembly on hydrophilic regions of self-assembled monolayers.

In the past few years, there has been a growing interest in using various external fields to manipulate bulk crystallization, with the expectation to ultimately control desired packing structures of PBG crystals.[8] The formation of colloidal crystals in bulk without the presence of external fields is now well understood. The disorder-to-order transition from the liquid to the solid state is mainly governed by thermal equilibrium.[9] For hard sphere systems, volume fraction is the only parameter that controls the phase transition.[10] Despite our understanding of bulk crystallization, questions concerning the influence of confining walls and additional external fields on colloidal matter still remain. The readers are referred to an excellent review given by Löwen on the recent discoveries of novel phase transition phenomena triggered or generated by the confining walls and external fields.[11] In general, packing structures through sedimentation depend largely on the dynamical behavior of colloidal particles and their interactions with imposed external fields. At the submicrometer scale, two important factors control particle dynamics of a colloidal system. One is the surface forces acting between two colloids and the other is the Brownian motion of colloids in a suspension.

Surface forces acting between two colloids originate from interatomic forces at the atomistic scale. These forces at the colloidal scale manifest themselves into various forms including electrostatic forces, van der Waals forces, salvation forces, steric forces, and hydrophobic and hydrophilic forces.[12] For a simple colloidal system without adsorbed substances (e.g., polymeric dispersants), van der Waals and electrostatic forces dominate.[12,13] These two forces can be characterized by the well-known Derjaguin–Landau–Verway–Overbeek (DLVO) theory[12–16] as the algebraic summation of electrostatic repulsion and van der Waals attraction.

Brownian motion of colloids in a suspension results from random collisions of solvent molecules acting on colloids. This actuation by solvent molecules is a major driving mechanism to ignite agglomeration in a suspension before particles deposit onto the substrate. Consequently, the effects have a profound impact on the packing structures. A conventional way to incorporate Brownian motion effects into a particle dynamics simulation is through the adoption of Brownian forces, which is characterized by suitable probabilistic distributions.[17,18]

Ansell and Dickinson's[19] pioneering work presented a simulation methodology to study sediment formation. Both colloidal interaction from the DLVO theory and diffusive characteristics of Brownian motion were considered. They concluded that packing structures were affected by both. However, their study was based on a scheme of single particle deposition that was meant to model an infinite dilute system. Particle agglomeration during the settling process was not taken into consideration. On the other hand, Hong[13] studied colloidal particle movement in a suspension and found that the surface potential of particles had a profound impact on the final packing structures. However, some of these packing results disagreed with the experimental observations.

In this paper, the packing history and packing structures of PBG crystals are studied with particle dynamics simulations and tailored experiments. We develop a simulation methodology in detail to describe the dynamical behavior of colloidal particles because of the combined actions of Brownian motion, inter-particle interactions, and imposed external fields. Simulations and experiments are conducted to examine particle agglomeration in a solution and its consequent effects on packing struc-

G. Franks—contributing editor

Manuscript No. 20811. Received July 28, 2005; approved November 11, 2005.
Presented at the 106th Annual Meeting of The American Ceramic Society, Indianapolis, Indiana, April 19, 2004 (Symposium 11, Photonics Materials and Devices, Paper No. AM-S11-41-2004).
Supported by the National Science Council of Taiwan, NSC 92-2211-E-002-081 and the National Center of High-Performance Computing of Taiwan.
*Member, American Ceramic Society.
†Author to whom correspondence should be addressed. e-mail: dchen@ntu.edu.tw

tures. Finally, simulations provide us with a gateway to study dynamical evolution from dispersed states in a solution to the final packing structures. The evolution of packing structures because of coupling between the inter-particle interactions and imposed external fields is also analyzed.

II. Experimental Procedure

(1) Preparation of Mono-Sized SiO_2 Particles

Tetra-ethyl orthosilicate (TEOS; MERCK-Schuchardt, Germany) in a purified grade and ammonia solution (ammonium hydroxide, 28–30 wt% solution of NH_3 in water, Acros Organics, NJ, USA) were used. Ethanol (extra pure reagent, 99.5%, Shimakyu Pure Chemicals, Osaka, Japan) and de-ionized water are the solvents. The detailed description of synthesis has been reported in our previous article.[20]

After washing three times with 95% pure ethanol and once with de-ionized water, the spherical SiO_2 particles were dispersed in the aqueous solution in which the electrolyte concentration was set at 0.001 M with NaCl. The concentration of SiO_2 in the aqueous solution was set at 5 wt%.

We manipulated the pH value to control inter-particle interactions that are a function of ζ potentials based upon the double-layer theory.[16,21] The pH value was adjusted to 2 or 10 with HCl and NaOH. From the isoelectric point (IEP) curve of amorphous silica, we found that the ζ potentials of SiO_2 particles are $\zeta = +5$ mV and $\zeta = -50$ mV for the condition of pH = 2 and pH = 10, respectively. Close to its IEP (at pH = 2.2), a particle has a weak repulsive potential and it is easy for it to aggregate with others. In contrast, a SiO_2 particle is likely to remain dispersed in the suspension at a pH value beyond its IEP because of a high surface charge. The container's material was borosilicate glass whose IEP is similar to that of colloidal silica. The contact effect of the container was thus ignored.

The SiO_2 sediment was prepared from the SiO_2 suspension by centrifuging with 550 *g* (3000 rpm) for 20 min in disposable culture tubes of borosilicate glass. The centrifuge machine was Laboratory Centrifuge Z380 (Berthold Hermle AG, Gosheim, Germany). The chosen centrifuging rate did not induce a change in the shape of the SiO_2 spheres but it did speed up the packing rate. The sample was dried at room temperature for 2 ~ 3 days, and then placed in an oven maintained at 105°C for 24 h. The sintering process was performed from room temperature to 500°C and then holding at 500°C for 4 h. The heating rate was 10°C/min. To characterize the size of the SiO_2 particles, a particle sizer (MASTER2000, Malvern, U.K.) and TEM (JEOL 100CXII, Akishima, Japan) were used. The morphologies of particles were observed by Field Emission SEM (Leo, Instrument 1530, Cambridge, U.K.). The size of the particles prepared for this study had been confirmed to be around 400 nm in diameter thereafter.

For the case of $\zeta = -50$ mV, we found that the particle size distribution at the beginning of the test and after 3-day sedimentation were almost identical, with a single sharp peak at 400 nm. From SEM observations, we found that the particles had a mono-size of about 400 nm. Thus, we concluded that the particles were well dispersed in the suspension through packing for this case.

For the case of $\zeta = +5$ mV, we first observed that all the particles quickly settled in 1 h during the tests. The particle size distributions for the initial state and for the state after 10 min of sedimentation were nearly identical, with a wider distribution and a peak at 1500 nm. This implies that the agglomerations occurred because of rapid Brownian coagulation and had reached a stable state in a very short period of time right after the initial state.

The SEM images of the packing structures are shown in Figs. 1(A) and (B). These morphologies are related to the cases of $\zeta = +5$ mV and $\zeta = -50$ mV, respectively. In the former, the image reveals a random arrangement on the surface of the centrifuged SiO_2 cake. The pore is likely caused by particle agglomeration in the suspension. The roughness of the surface is about five to ten times the size of SiO_2 particles. In the latter, a well-packed structure on the surface of the SiO_2 centrifuged cake can be observed. Despite the presence of a few vacancies, faults, and domain boundaries, most of particles were arranged in a close-packed manner. The surface roughness was about the size of the SiO_2 particles.

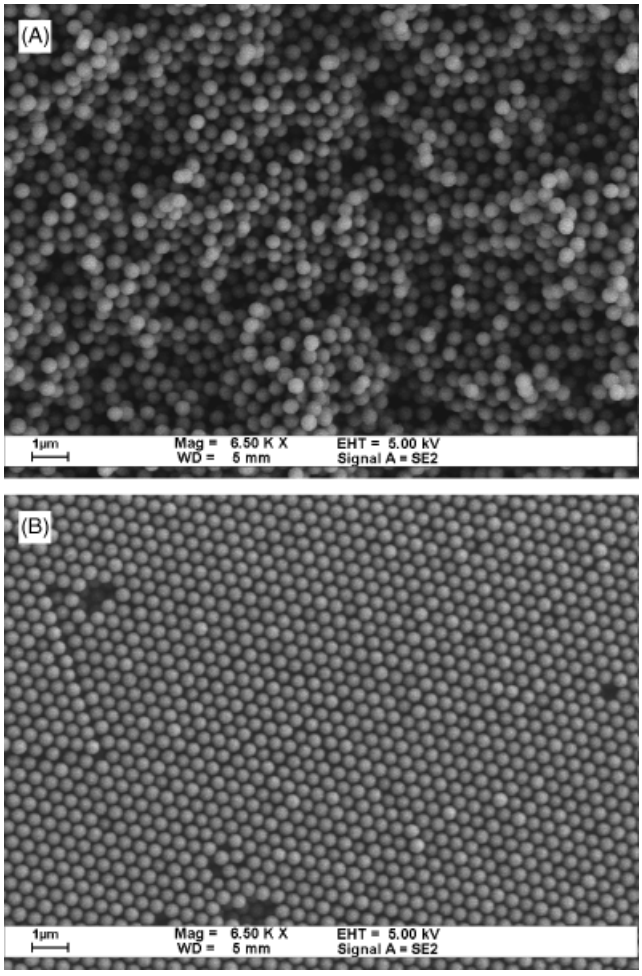

Fig. 1. (A) SEM images of SiO_2 packing structures for the case of $\zeta = +5$ mV. (B) SEM images of SiO_2 packing structures for the case of $\zeta = -50$ mV.

III. Simulation

(1) Equation of Motion

The movement of a colloidal particle in a suspension is governed by Newtonian dynamics where forces include those from inter-particle interactions of its neighboring particles, solutions and imposed fields, and collisions of solvent molecules acting on the particles. From the Langevin equation, the balance equation of motion for a particle in a suspension can be expressed as[17]

$$m\dot{\mathbf{v}} + 6\pi\eta r\mathbf{v} = \mathbf{F} + \mathbf{X} \tag{1}$$

in which m is the mass of the particle, $\mathbf{v}$ the velocity vector of the particle, η the viscosity of the medium, r the radius of the particle, $\mathbf{F}$ the external force vector that includes the contribution from field forces and inter-particle forces, and $\mathbf{X}$ the random force vector that represents the stochastic nature of a force activated by the medium's molecules. At a specific time t, given that all the external forces can be treated constantly during a small incremental time step Δt, the position of the particle

at the next time step $t + \Delta t$ can be obtained by the following equation[17]

$$\mathbf{r}(t+\Delta t) = \mathbf{r}(t) + \frac{\mathbf{v}(t)}{\beta}(1 - e^{-\beta\Delta t}) + \frac{\mathbf{F}(t)}{m\beta} \times \left[t - \frac{1}{\beta}(1 - e^{-\beta\Delta t})\right] + \mathbf{R}(\Delta t) \quad (2)$$

in which $\beta = 6\pi\eta r/m$, $\mathbf{F}(t)$ is the summation of all external force vectors imposed on the particle at time t, and $\mathbf{R}(\Delta t)$ is a stochastic term that represents the displacement vector of Brownian motion during the time increment Δt.

It is noteworthy that β^{-1} represents the relaxation time. Thus, for the diffusive time scale in which $\Delta t >> \beta^{-1}$, each component of $\mathbf{R}(\Delta t)$ can be specified as a function of the first and second probability moments of a Gaussian distribution[9]:

$$\mu = \langle R(\Delta t)\rangle = 0 \quad (3)$$

$$\sigma^2 = \langle R_i(\Delta t) R_j(\Delta t)\rangle = 2D_{ij}\Delta t \quad (4)$$

in which D_{ij} is the diffusion tensor for the focused particle i and neighboring particles j in the suspension. As the primary interest in this study is the structures of sedimentation, D_{ij} can be further simplified using the Stokes–Einstein diffusion coefficient D_0.[19] Equation (4) thus reduces to

$$\sigma^2 = \langle R_i(\Delta t) R_j(\Delta t)\rangle = 2D_0\Delta t \quad (5)$$

in which $D_0 = k_B T/6\pi\eta r$ where k_B is the Boltzmann constant and T the temperature in Kelvins.

At the range from a few nanometers to a micron, the inter-particle interactions can be characterized by the DLVO theory[12,16,21]

$$V_{DLVO} = V_{vdw} + V_{ele} \quad (6)$$

in which V_{vdw} denotes the van der Waals energy, V_{ele} denotes the electrostatic repulsive energy, and V_{DLVO} denotes the total DLVO potential energy, respectively. For the interaction between two spherical particles, the van der Waals and electrostatic potentials can be expressed as[9,12,13]

$$V_{vdw} = -\frac{A_H}{6}\left[\frac{2r_1r_2}{d^2-(r_1+r_2)^2} + \frac{2r_1r_2}{d^2-(r_1+r_2)^2+4r_1r_2} + \ln\left(\frac{d^2-(r_1+r_2)^2}{d^2-(r_1+r_2)^2+4r_1r_2}\right)\right] \quad (7)$$

$$V_{ele} = 64\pi\varepsilon_r\varepsilon_o\left(\frac{RT}{zF}\right)^2 \times \tanh\left(\frac{zF\zeta_1}{4RT}\right) \times \tanh\left(\frac{zF\zeta_2}{4RT}\right) \times \frac{r_1r_2}{r_1+r_2}e^{-\kappa h} \quad (8)$$

in which h is the surface separation distance and d the center-to-center distance between two objects, A_H is the Hamaker constant, ζ_1 and ζ_2 are the ζ-potentials, κ is the Debye–Huckel parameter where κ^{-1} represents the characteristic thickness of the double layer, F is the Faraday constant, z the valence of the electrolyte, ε_r the dielectric constant of the medium, ε_0 the permittivity of vacuum, and R the gas constant, respectively.

For the interaction between a spherical particle and a boundary plate, the van der Waals energy can be expressed by setting $r_1 = r$ and taking the limit as $r_2 \to \infty$. We thus obtain

$$V^b_{vdw} = -\frac{A_H}{6}\left[1 + \frac{h}{2r+h} + \frac{h}{r}\ln\left(\frac{h}{2r+h}\right)\right] \quad (9)$$

Ives and Gregory proposed that the electrostatic potential between the spherical and planar geometries can be expressed as follows[16,22]

$$V^b_{ele} = 9.24\times10^{-11} r \times \tanh\left(\frac{zF\zeta_1}{4RT}\right) \times \tanh\left(\frac{zF\zeta_2}{4RT}\right) \times \ln(1+e^{-\kappa h}) \quad (10)$$

Furthermore, the DLVO potential energy can be transformed into the force fields by the differentiation of the potential energy with respect to the surface separation distance h:

$$F_{DLVO} = \frac{\partial V_{DLVO}}{\partial h} = F_{vdw} + F_{ele} \quad (11)$$

in which F_{vdw} denotes the van der Waals attractive force, F_{ele} denotes the electrostatic force, and F_{DLVO} denotes the total DLVO force, respectively. For the interaction between two spherical particles, these forces can be expressed as

$$F_{vdw} = -\frac{A_H(4r_1r_2)^3}{6} \times \left[\frac{d}{\left[d^2-(r_1+r_2)^2\right]^2 \times \left[d^2-(r_1+r_2)^2+4r_1r_2\right]^2}\right] \quad (12)$$

$$F_{ele} = 64\pi\varepsilon_r\varepsilon_0\kappa\left(\frac{RT}{zF}\right)^2 \times \tanh\left(\frac{zF\zeta_1}{4RT}\right) \times \tanh\left(\frac{zF\zeta_2}{4RT}\right) \times \frac{r_1r_2}{r_1+r_2}e^{-\kappa h} \quad (13)$$

For the interaction between a spherical particle and a boundary plate, these forces can be expressed as

$$F^b_{vdw} = -\frac{2A_H r^3}{3[(d-r)\times(d+r)]^2} \quad (14)$$

$$F^b_{ele} = \frac{9.24\times10^{-11}\kappa r\left(\frac{RT}{zF}\right)^2 \times \tanh\left(\frac{zF\zeta_1}{4RT}\right) \times \tanh\left(\frac{zF\zeta_2}{4RT}\right) \times e^{-\kappa h}}{1+e^{-\kappa h}} \quad (15)$$

To avoid numerical singularity while computing the DLVO interaction close to contact, the Johnson–Kendall–Roberts (JKR) adhesive model is applied.[23] At this very short range (less than 0.4 nm approximately to contact physically), surface adhesion keeps the particles in contact. For two elastic spheres, the adhesive force F_{JKR} based upon the JKR theory with deformable modification of the Derjaguin approximation can be described as follows[23,24]

$$F_{JKR} = \frac{3\pi}{2}\frac{r_1r_2}{r_1+r_2}W_{1L2} \quad (16)$$

in which W_{1L2} is the effective work of adhesion (per unit area). This work can be determined by the specific surface energies γ_{ij}[16,21]:

$$W_{1L2} = \gamma_{12} - \gamma_{1L} - \gamma_{2L} \quad (17)$$

where the subscripts 1, 2, and L represent the two particles in contact and the medium, respectively. When two particles come to the distance of solid contact, a simple linear spring model is used to keep the particles free from geometrical overlapping.

In summary, all the inter-particle forces mentioned above versus the surface separation distance between two particles are plotted in Fig. 2. At the long range, an energy barrier resulting

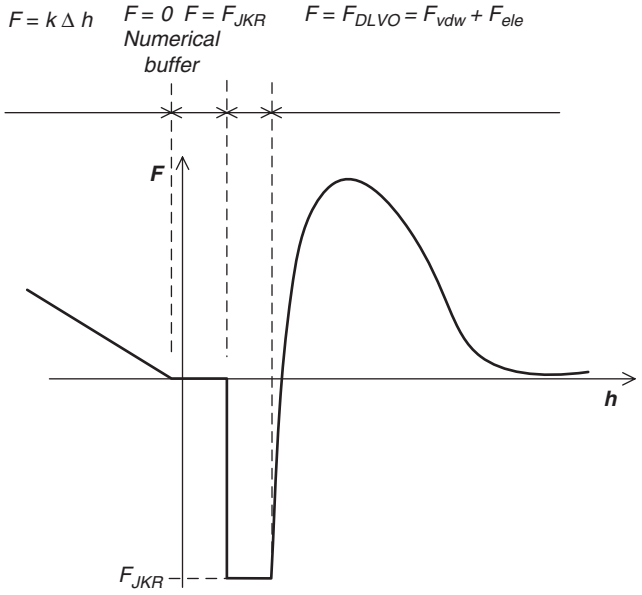

Fig. 2. Inter-particle interaction mechanism—force (F) versus separation (h) curve.

from the DLVO theory maintains stability that keeps two colloidal particles from agglomeration. Once the particles overcome the repulsive barrier, an irreversible attraction occurs. The attractive force increases as the separation distance decreases until its magnitude is equal to the adhesive force, F_{JKR}. Afterwards, a constant F_{JKR} takes over to attract the particle until the particles come into solid contact where a simple spring model is then used. Finally, a zero-force buffer zone of about 0.2 nm was introduced in the simulation to shorten the uninteresting but time-consuming balancing process.

(2) Simulation Parameters

From the IEP curve of SiO_2, the ζ potentials of SiO_2 particles are $\zeta = +5$ mV and $\zeta = -50$ mV for the condition of pH = 2 and pH = 10, respectively. Other simulation parameters are determined based on the experimental conditions listed in Table I. The inverse Debye screening length in the solution of NaCl electrolyte is obtained by[9,12]:

$$\kappa = \sqrt{\frac{2e^2 C N_A}{\varepsilon_0 \varepsilon_r k_B T}} \tag{18}$$

where e is the charge on the electron, N_A the Avogadro's number, and C the ionic strength. The corresponding DLVO interaction curves for $\zeta = +5$ mV and $\zeta = -50$ mV are plotted

Table I. Simulation Parameters

Particles (SiO_2)	Value
Radius (r)	200 nm
Density (ρ)	2.2×10^3 kg/m^3
Hamaker constant (A_H)	1.51×10^{-20} J
Zeta potential (ζ)	+5, −50 mV
Density (ρ) of medium (water)	1×10^3 kg/m^3
Viscosity (η) of medium	1×10^{-3} Pa · s
Temperature (T)	300°K
Dielectric constant (ε_r) of medium	80.1
Ionic strength (NaCl) (C)	0.001 M
Debye screening length (κ^{-1})	10 nm
Ionic valence (z)	1

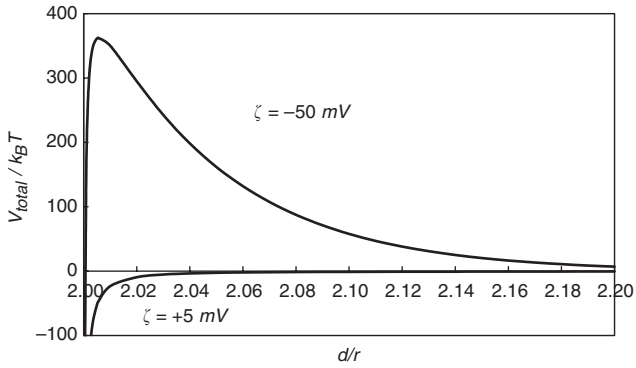

Fig. 3. Dimensionless Derjaguin–Landau–Verway–Overbeek (DLVO) interaction for the cases of $\zeta = +5$ mV and $\zeta = -50$ mV. V_{total} is the DLVO potential, d is the center-to-center distance between two particles, and r is the radius of the particle.

in Fig. 3. An observation can be made from the figure that the energy barrier of DLVO repulsion for the case of $\zeta = -50$ mV is about 350 times $k_B T$, which represents the energy of Brownian motion. On the other hand, the attractive potential dominates the interactions for the case of $\zeta = +5$ mV.

(3) Particle Agglomeration

Particles might agglomerate in the solution. In this study, it is assumed that the agglomerated particles in a cluster move together in the same direction and magnitude under Brownian dynamics. Thus, for a given time increment when Brownian motion is applicable, it is necessary to identify a set of clusters, each consisting of agglomerated particles. In addition, we need to compute the effective radius for each cluster to perform proper sampling for Brownian motion.

The characteristics of the DVLO interaction are used to identify the cluster. As illustrated in Fig. 4, particles will form a cluster if the separation distance between them is smaller than a specific value, h_b. This value is the separation distance that signifies the beginning of irreversible attraction. Once the cluster is formed, its effective radius needs to be determined to sample the corresponding Brownian movement. In this study, the effective radius illustrated in Fig. 4 is computed through an equivalent mass model:

$$r_{eff} = \sqrt[3]{\frac{3 \times \sum_{i=1}^{M} m_i}{4\pi\rho}} \tag{19}$$

in which M is the number of particles in the cluster and ρ is the density of the particle.

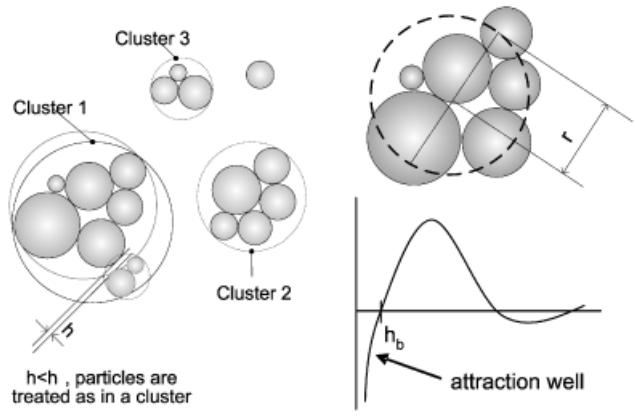

Fig. 4. Illustration of cluster formation and the effective radius of a cluster.

Last but not the least, because the sampling for each particle or cluster is randomly selected, it is possible to introduce geometrical overlapping between particles during the simulation. This overlapping obviously violates the physical phenomena and should be modified accordingly. A simple strategy is used in this study in which the contribution from Brownian motion was ignored for a given time increment if overlapping persists on the second trial of random movement. More sophisticated strategies were performed in our previous study.[25] Nevertheless, no quantitative difference was found for the long-term agglomeration status when different strategies were used.

(4) Model Geometry and Initial Condition

The container used in the experiments was a few centimeters in size while the size of particles before agglomeration was about 400 nm. This vast difference in the length scale prevented the direct construction of a full-scale model for the simulation. As we were primarily interested in studying final packing structures, we assumed that an intermediate state existed in the experiments. Such a state allows the construction of a rational initial model for the simulation. The insights gained from the particle size distribution analysis in the experiment allow the setup of proper initial models. A box 12 μm on both sides and 8 μm height containing 4500 particles was constructed. Periodical boundary conditions were assigned on four sides, and fixed and free boundary conditions were assigned on the top and bottom faces of the box. For the case of $\zeta = +5$ mV, the initial agglomerated states were assigned based on the size distribution of particle sizer observation, and are listed in Table II. For the case of $\zeta = -50$ mV, particles were randomly dispersed in the box.

(5) Simulation Process

Adopting a proper incremental time step is crucial for the simulation. If the increment is too large, it might result in large particle displacements and may lead to an unrealistic deep contact between particles. Consequently, this penetration may cause the simulation system to become unstable. In contrast, if the time increment is too small, it may take an enormous computing time to finish the simulation. Based on our experience, a heuristic rule of thumb to select a proper time step increment is to control the displacement within the order of hundredth of the particle size. This corresponds to the scale of 10^{-9} m in our simulation.

After several preliminary runs, we found that the velocity of the particles was within the order of 10^{-2} m/s. Therefore, choosing $\Delta t = 10^{-7}$s for the deterministic movement in Eq. (2) is proper. As the particle displacement is the algebraic summation of deterministic and stochastic movements, the time step used for Brownian motion can be different from the deterministic part. By choosing $\Delta t = 10^{-6}$s, the standard deviation of Brownian motion from Eq. (5) can be controlled at the order of 10^{-9} m. Consequently, we perform Brownian motion sampling in every ten increments in the simulation.

The packing process involved two-stage modeling. The first simulated the consolidation process and the second simulated the drying process of a sediment cake in experiments. We monitored the total elevation of each particle in the system to identify the termination criterion for the first stage. The total elevation potential can be expressed as

$$\sum_{i=1}^{N} mg\hat{h}_i \tag{20}$$

where g is the gravity, $\hat{h}$ the elevation measured from the centroid of a particle to the substrate, and N is the total number of

Table II. Initial Cluster Distribution for the Case of $\zeta = +5$ mV

Particles in cluster	No. of clusters	No. of particles	Percentage (%)
1	25	25	0.6
3	80	240	5.3
15	125	1875	41.7
80	17	1360	30.2
500	2	1000	22.2
Total		4500	100

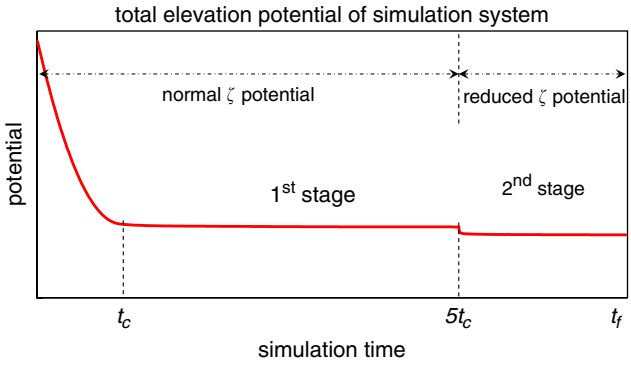

Fig. 5. Illustration of time history of the total elevation potential through the first and second stages of packing simulation.

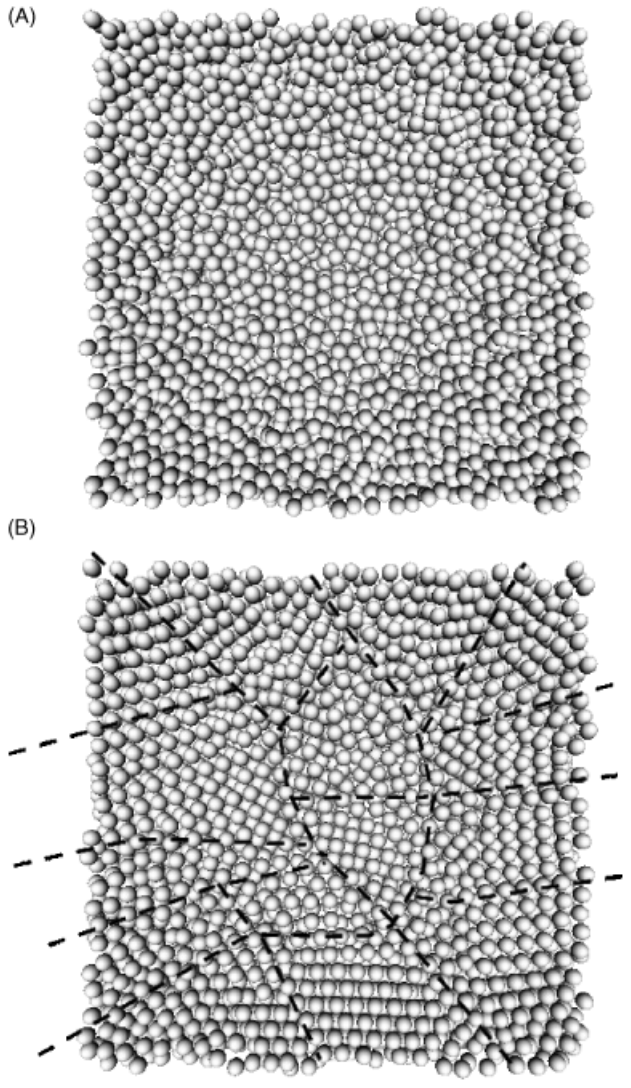

Fig. 6. (A) Final stage of simulation packing structures for the case of $\zeta = +5$ mV. (B) Demonstration of particles and domain boundaries for the case of $\zeta = -50$ mV in the final stage.

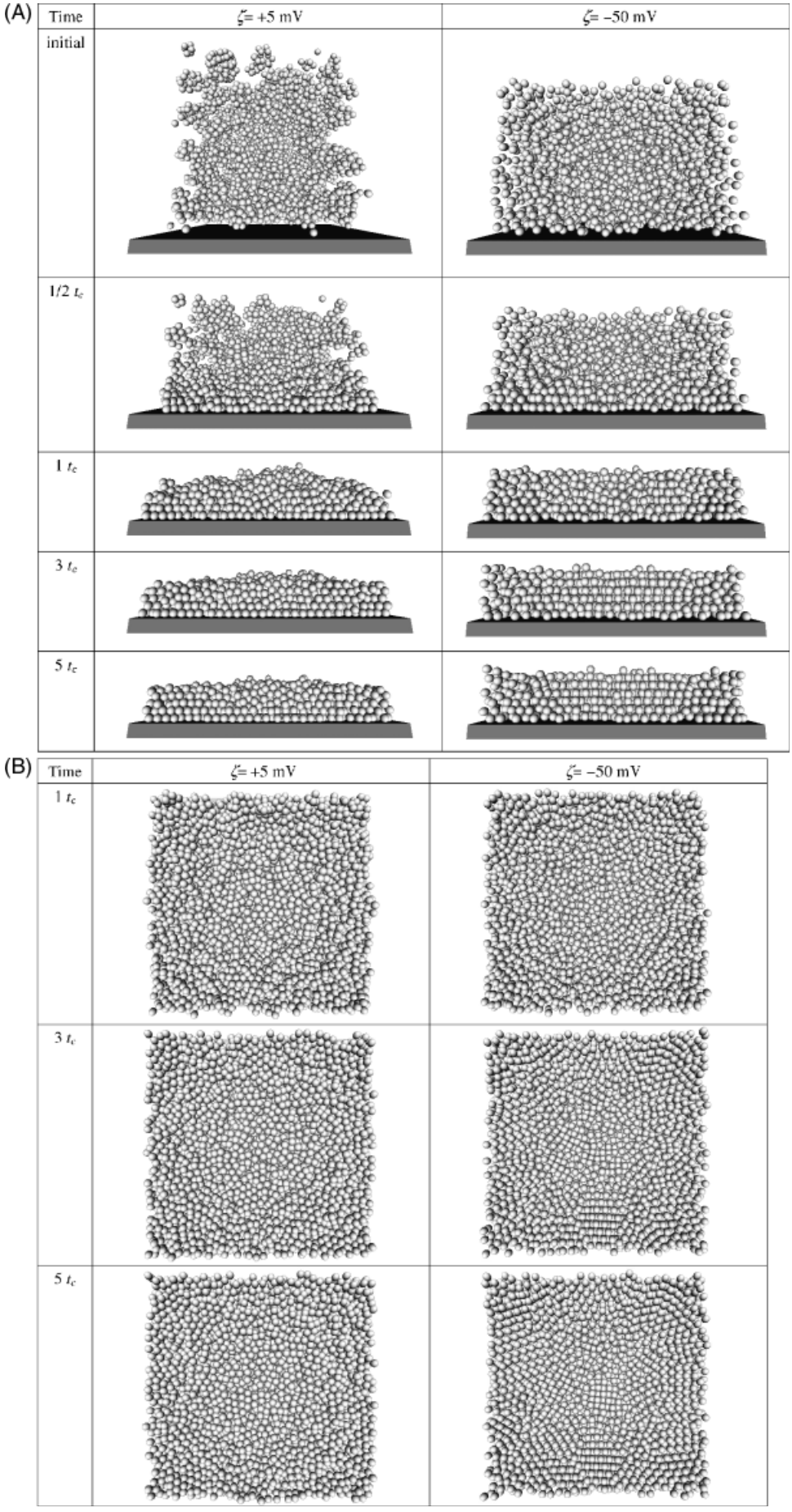

Fig. 7. (A) Side view through the packing process for the cases of $\zeta = +5$ mV and $\zeta = -50$ mV. (B) The top view through the packing process for the cases of $\zeta = +5$ mV and $\zeta = -50$ mV. (C) The bottom layer through the packing process for the cases of $\zeta = +5$ mV and $\zeta = -50$ mV.

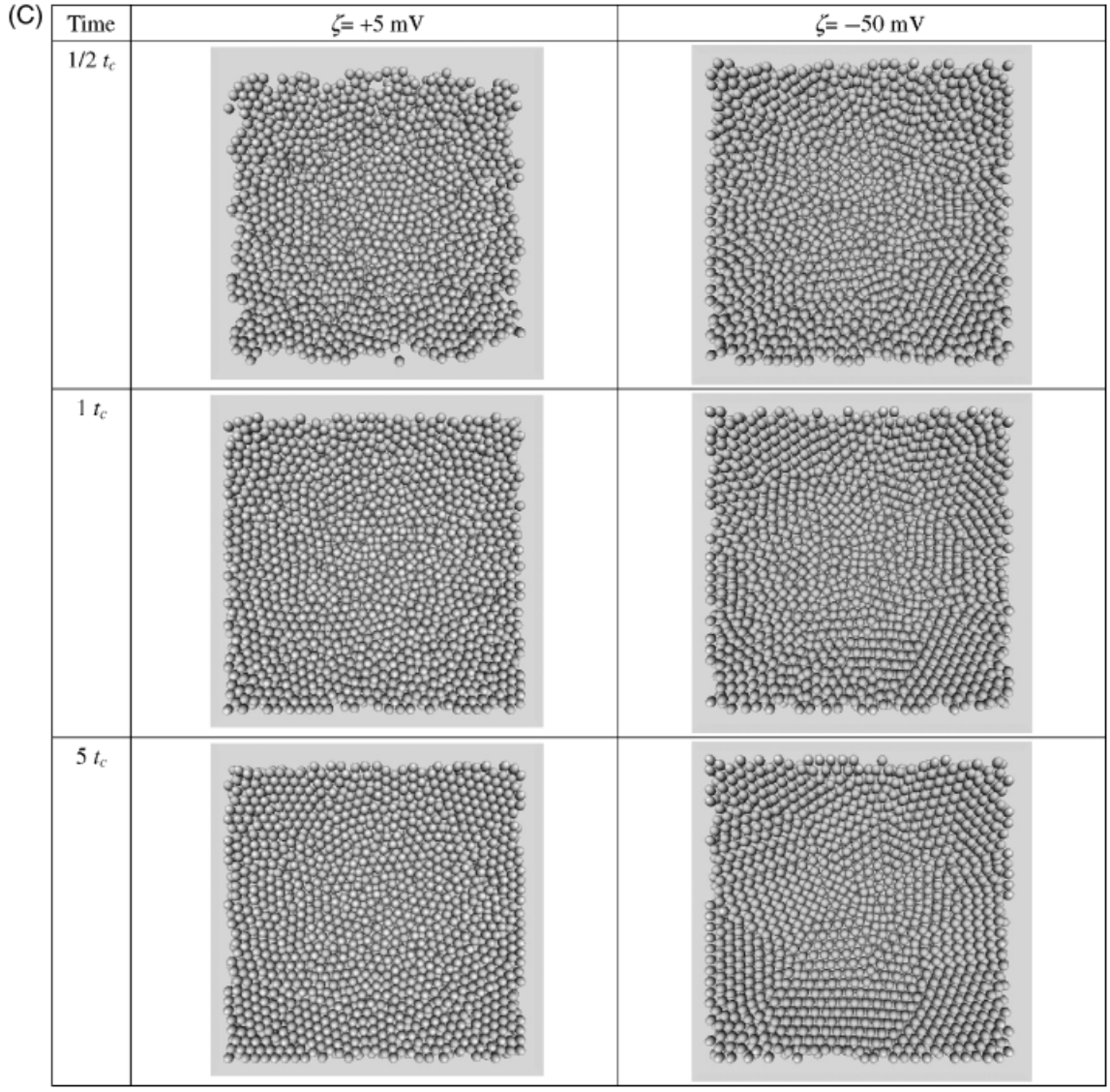

Fig. 7. Continued.

the particles. The elevation potential will eventually reach a stable state, as illustrated in Fig. 5. In this study, we defined the consolidated time (t_c) to be the moment when the difference of the elevation potential between two consecutive increments is less than 0.1%. Although the thickness of the sediment cake will no longer change by time t_c, particles inside the sediment will continue to rearrange themselves. As shown later in the numerical results, this dynamical rearrangement reached a balancing state at about 4–5t_c. Thus, the first stage of packing simulation was terminated at 5t_c.

The second stage of packing simulation corresponded to the drying process in the experiments. In this process, the water between particles was expelled on drying. Consequently, the surface tension induced by the capillary force between particles increased to attract the particles. Detailed simulations of this process such as consideration of the vertical gradient of water concentration arising from the drying are beyond the scope of this paper, and are the subject of future investigations. In this study, once the packing simulation reached its first stage, we gradually reduced the ζ potential of the particles to mimic the surface tension effect until the total elevation potential of the system reached another plateau at t_f. This simplified approach is thus likely to scale the spatial structures uniformly from the first stage.

The procedures mentioned above concluded our two-stage packing simulation. A typical run of these simulations took about 70 000 time increments and about a week to complete a run in an Intel P4 2.26 GHz machine with 1.0 GB of RAM.

IV. Simulation Results and Discussion

The final packing structure at t_f from the simulation for the case of $\zeta = +5$ mV is shown in Fig. 6(A). It reveals an irregular packing surface similar to those observed in the experiments. We can estimate that the roughness was about five times the particle size. No regularity of particle arrangements was found on the surface. The final packing structure at t_f from the simulation for the case of $\zeta = -50$ mV is shown in Fig. 6(B). The surface profile is rather smooth. It also reveals the combination of several recognizable domain structures. Most close-packed structures were formed inside a domain, and cubic packing (or disordered arrangements) was formed near the boundary. Some disorder of particle arrangements corresponded to vacancies or flaws. In comparison with the experimental results, the ordered domain size was relatively small. Meanwhile, disorder between domains occurred more frequently than that in the experiments. These artifacts were likely caused by the finite size effects in the simulation models or limited time effects in the simulation process. Generally speaking, the simulation results agree with the experimental observations.

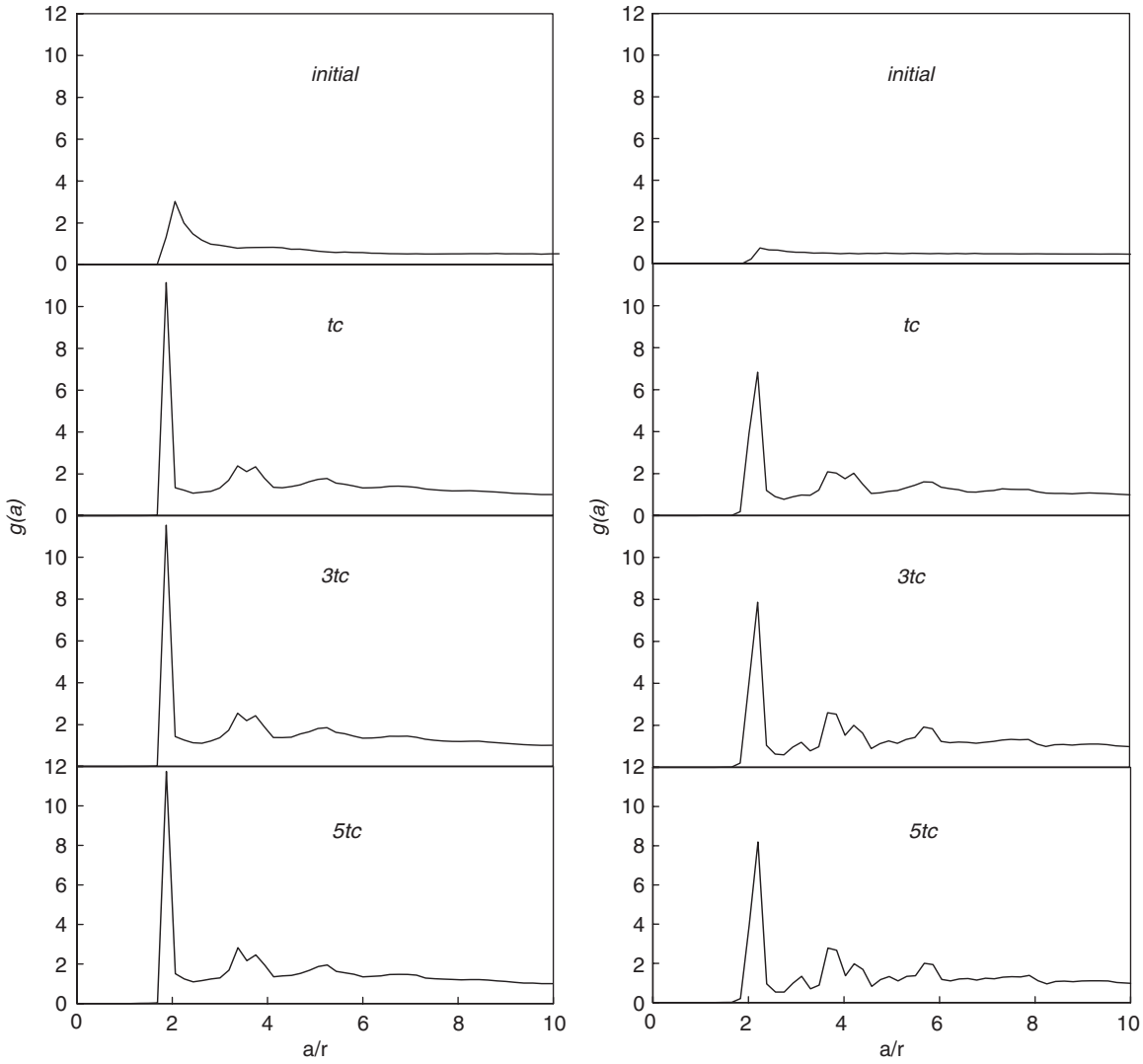

Fig. 8. Radial distribution function for the cases of $\zeta = +5$ mV and $\zeta = -50$ mV.

Next, we studied the evolution of packing structures during the simulation. As the packing structure at $5t_c$ and t_f for both cases was scaled proportionally, only the pattern growth from the initial state to $5t_c$ was studied. The evolutions of packing structures from the simulation for the case of $\zeta = +5$ mV and $\zeta = -50$ mV are shown in Figs. 7(A), (B), and (C). From the initial state to t_c, the differences of surface profiles between the cases of $\zeta = +5$ mV and $\zeta = -50$ mV were clearly observed. From t_c to $5t_c$, particles continued adjusting their positions in both cases. Nevertheless, only the case of $\zeta = -50$ mV, in which highly repulsive forces persisted between particles, gradually formed regular close-packed structures. More interestingly, comparison of Fig. 7(B) with Fig. 7(C) revealed that regularity occurred much earlier at the bottom layer. This phenomenon might have occurred because of the constraint effects. In comparison with the particles situated at the top layer, the movements of particles at the bottom layer were constrained by the increase of the centrifugal forces as well as the fixity of the substrate. These constraints, together with persistent repulsive forces between particles, shaped the pattern formation at the bottom layer and led to emergence of regularity gradually toward the top layer. Finally, the similarity of pattern arrangements between the bottom and the top layers also suggests an upward pattern growth mechanism from the substrate. This observation provides a future gateway to engineer desired substrate templates for manipulating pattern formation on the surface.

We also performed the radial distribution function (RDF) analysis in the sediment cake to retrieve alignment information of packing structures. The RDF is a common way to measure how particles organize themselves around each other.[26] This function $g(a)$ describes the probability of finding a particle a distance a from another particle compared with the ideal gas distribution:

$$g(a) = \frac{\langle N(a,\ \Delta a)\rangle}{\frac{1}{2}N\tilde{\rho}V(a,\ \Delta a)} \tag{21}$$

where N is the total number of particles, $N(a, \Delta a)$ is the number of particles found in a spherical shell of radius a and thickness Δa, $V(a, \Delta a)$ is the volume of the spherical shell, and $\tilde{\rho}$ is the number of particles in a unit volume.

The RDF plots for both cases are shown in Fig. 8. For the case of $\zeta = +5$ mV, the initial RDF showed a liquid-like state. This distribution changed into a solid state with a high peak at $a/r = 2$. The similarity between the RDF plots at t_c, $3t_c$, and $5t_c$ provides further evidence that no patterns were formed in this case. For the case of $\zeta = -50$ mV, the initial RDF shows a gas-like state. This distribution again changed to a solid state with a high peak at $a/r = 2$. The peaks of the RDF distribution at t_c are as ambiguous as those of $\zeta = +5$ mV. However, the peaks gradually became apparent at $3t_c$ and $5t_c$. This echoed the observations made above in which the regularity of the packing patterns had been gradually shaped from t_c to $5t_c$ in this case.

V. Conclusions

We have presented a particle dynamics simulation methodology to model the packing history and packing structures of PBG crystals, and conducted tailored experiments to support our simulation results. From the results reported herein, three major concluding remarks can be drawn. Firstly, particles inside a sediment cake continue adjusting their positions by inter-particle interactions even after the height of the cake has reached a stable condition. However, only the case with the persistence of highly repulsive forces between particles gradually forms regular close-packed structures. Secondly, from cross-sectional analysis of the top and bottom layers and from the RDF analysis, we have observed that the desired close-packed patterns on the surface are propagated from those at the bottom layer during the consolidation. The major driving forces for the pattern formation and growth are the coupling between inter-particle interactions and constraints from imposed external fields. Finally, agglomerates with weak repulsive forces in the solution because of rapid Brownian coagulation tend to retain similar random packing states through the consolidation and drying stages.

References

[1]J. Joannopoulos, R. D. Meade, and J. N. Winn, *Photonic Crystals: Molding the Flow of Light*. Princeton University Press, Princeton, NJ, 1995.

[2]J. Ballato and A. James, "A Ceramic Photonic Crystal Temperature Sensor," *J. Am. Ceram. Soc*., **82** (8) 2273–5 (1999).

[3]P. V. Braun, R. W. Zehner, C. A. White, M. K. Weldon, C. Kloc, S. Patel, and P. Wiltzius, "Epitaxial Growth of High Dielectric Contrast Three-Dimensional Photonic Crystals," *Adv. Mater*., **13** (10) 721–4 (2001).

[4]P. D. Rack, A. Namam, P. H. Holloway, S.-S. Sun, and R. T. Tuenge, "Materials Used in Electroluminescent Display," *MRS Bull*., **21** (3) (March) 49–58 (1996).

[5]M. Trau, D. A. Saville, and I. A. Aksay, "Field-Induced Layering of Colloidal Crystals," *Science*, **272** (5262) 706–9 (1996).

[6]P. Sarkar, D. De, K. Yamashita, P. S. Nicholson, and T. Umegaki, "Mimicking Nanometer Atomic Processes on a Micrometer Scale via Electrophoretic Deposition," *J. Am. Ceram. Soc*., **83** (6) 1399–401 (2000).

[7]Y. Masuda, K. Tomimoto, and K. Koumoto, "Two-Dimensional Self-Assembly of Spherical Particles Using a Liquid Mold and Its Drying Process," *Langmuir*, **19** (13) 5179–83 (2003).

[8]A.van Blaaderen, "Colloids Under External Control," *MRS Bull*., **29** (2) (February) 85–90 (2004).

[9]W. B. Russel, D. A. Saville, and W. R. Schowalter, *Colloidal Dispersions*. Cambridge University Press, Cambridge, 1989.

[10]H. Löwen, "Fun with Hard Spheres"; pp. 295–331 in *Lecture Notes in Physics 554*, Edited by K. R. Mecke and D. Stoyan, Springer-Verlag, Berlin, 2000.

[11]H. Löwen, "Colloidal Soft Matter under External Control," *J. Phys: Condens. Matter*, **13**, R415–32 (2001).

[12]R. G. Horn, "Surface Forces and Their Action in Ceramic Materials," *J. Am. Ceram. Soc*., **73** (5) 1117–35 (1990).

[13]C. W. Hong, "New Concept for Simulating Particle Packing in Colloidal Forming Processes," *J. Am. Ceram. Soc*., **80** (10) 2517–24 (1997).

[14]B. Derjaguin and L. Landau, "Theory of the Stability of Strongly Charged Lyophobic Sols and of the Adhesion of Strongly Charged Particles in Solutions of Electrolytes," *Actz. Physicochim*., **14**, 663–662 (1941).

[15]E. J. W. Verwey and J. Th. G. Overbeek, *Theory of the Stability of Lyophobic Colloids*. Elsevier, Amsterdam, 1948.

[16]R. J. Hunter, *Foundations of Colloid Science*, 2nd edition, Oxford University Press, New York, 2001.

[17]D. L. Ermak and H. Buckholz, "Numerical Integration of the Langevin Equation: Monte Carlo Simulation," *J. Comput. Phys*., **35**, 169–82 (1979).

[18]H. Markus, "Brownian Dynamics Simulation of Stable and of Coagulating Colloids in Aqueous Suspension", PhD dissertation, Swiss Federal Institute of Technology, Zurich, 1999.

[19]G. C. Ansell and E. Dickinson, "Sediment Formation by Brownian Dynamics Simulation: Effect of Colloidal and Hydrodynamic Interactions on the Sediment Structure," *J. Chem. Phys*., **85** (7) 4079–86 (1986).

[20]J. T.-W. Chen and W. J. Wei, "Synthesis and Characterization of Mono-Sized SiO_2 Ceramic Particles in Meso-Structure," *Ceram. Nanomat'ls Nanotech., Ceram. Trans*., **137**, 23–31 (2001).

[21]P. C. Hiemenz, *Principles of Colloid and Surface Chemistry*, 3rd edition, Marcel Dekker, New York, 1997.

[22]K. J. Ives and J. Gregory, "Surface Forces in Filtration," *Proc. Soc. Water Treatment Examination*, **15**, 93–116 (1966).

[23]C. W. Hong, "From Long-Range Interaction to Solid-Body Contact Between Colloidal Surfaces During Forming," *J. Eur. Ceram. Soc*., **18** (14) 2159–67 (1998).

[24]B. V. Derjaguin, "Untersuchungen uber die Reibung und Adhasion, IV: Theorie des Anhaftens kleiner Teilchen," *Kolloid Zeitschrift*, **69** (2) 155–64 (1934).

[25]J.-F. Li, W.-H. Yu, C.-S. Chen, and W.-C. J. Wei, "Modeling Nanosized Colloidal Particle Interactions with Brownian Dynamics Using Discrete Element Method", Nanotech 2003, pp. 566–9, [February], San Francisco, USA, 2003.

[26]J. M. Haile, *Molecular Dynamics Simulation: Elementary Methods*. John Wiley & Sons Inc., 1992. □

Copyright of Journal of the American Ceramic Society is the property of Blackwell Publishing Limited and its content may not be copied or emailed to multiple sites or posted to a listserv without the copyright holder's express written permission. However, users may print, download, or email articles for individual use.